Onset of Edge Wave Breaking in an Idealized Model of the Polar Stratospheric Vortex

XIAOHONG WANG

Department of Computer Science, University of Victoria, Victoria, British Columbia, Canada

JOHN FYFE

Canadian Centre for Climate Modelling and Analysis, Atmospheric Environment Service, University of Victoria, Victoria, British Columbia, Canada

(Manuscript received 4 December 1998, in final form 6 May 1999)

ABSTRACT

A mechanism for the breakdown of vertically propagating edge waves in a Boussinesq fluid is investigated within the context of the destruction of the polar stratospheric vortex. Under inviscid, quasi-linear, and slowly varying conditions in a three-dimensional, quasigeostrophic contour dynamics model it is analytically predicted that planetary-scale edge wave breaking will occur if the zonal mean flow is decelerated by more than approximately one-half its initial value via a positive group-velocity–mean-flow feedback mechanism. Fully nonlinear model simulations confirm this ''one-half rule'' and detail the sequence of events leading to the breaking.

1. Introduction

Fyfe and Held (1990, hereafter FH) investigated the interaction of equatorward-propagating Rossby waves and zonal mean flows, where the latter were initially free of any critical lines. For zonal mean flows containing a critical line it has been amply demonstrated that wave breaking will occur in the vicinity of the critical level (Warn and Warn 1976, 1978; Killworth and McIntyre 1985). The question addressed in FH was whether wave breaking can occur without a critical line (as often appears the case in the real atmosphere). In FH a stationary Rossby wave, sinusoidal in longitude, was slowly switched on, and the meridional propagation of the resulting wave front was examined. It was shown analytically that under inviscid, quasi-linear, and slowly varying conditions a steady state was obtained if, and only if, the zonal mean flow was decelerated by less than two-fifths of its initial value as a result of the passage of the wave front. Quasi-linear numerical simulations revealed that larger than ''two-fifths'' decelerations lead to critical-level formation followed by immediate wave breaking.

The physical explanation for this behavior is as follows. The passing wave front causes a mean-flow deceleration that acts to reduce the group velocity, and especially so in regions where the winds are the weakest. For a steady state to emerge, the wave activity must increase proportionately to the decrease in group velocity so that there will be no prolonged convergence of wave activity into these regions. However, when the two-fifths rule is violated this does not happen and the zonal-mean-flow deceleration and wave activity pileup continues unabated until, as the numerical simulations show, a critical level is formed.

Figure 1 illustrates graphically the mathematical basis of FH's two-fifths rule for Rossby wave breaking. The curves represent the relationship between wave activity density A and zonal mean flow $\overline{u}$ in the steady state for different forcing amplitudes η (with the functional dependence following from the fact that the group velocity varies inversely with A). The straight line represents the relation between A and $\overline{u}$ that exists at all times for flows evolving from initial zonal mean flow $\overline{u}^\circ$. Intersections between the straight line and the curves represent possible steady states for the given η and $\overline{u}^\circ$. It is evident from Fig. 1 that there exists a critical forcing denoted η^c (corresponding to the dashed curve) beyond which no steady states exist for the given $\overline{u}^\circ$. Corresponding to this critical forcing, there is a corresponding critical wave activity density A^c and zonal mean flow $\overline{u}^c$. Fyfe and Held (1990) showed that $A^c = 2\overline{u}^\circ/5$ and $\overline{u}^c = 3\overline{u}^\circ/5$, which are the basis of the two-fifths rule.

As stated, FH's investigation dealt with equatorward-propagating Rossby waves. In this investigation we consider vertically propagating planetary-scale ''edge waves.'' In this context, edge wave refers to a class of

Corresponding author address: John Fyfe, Canadian Centre for Climate Modelling and Analysis, University of Victoria, P.O. Box 1700, MS 3339, Victoria, BC V8W 2Y2, Canada.
E-mail: john.fyfe@ec.gc.ca

© 2000 American Meteorological Society

Unauthenticated | Downloaded 03/07/21 12:33 AM UTC

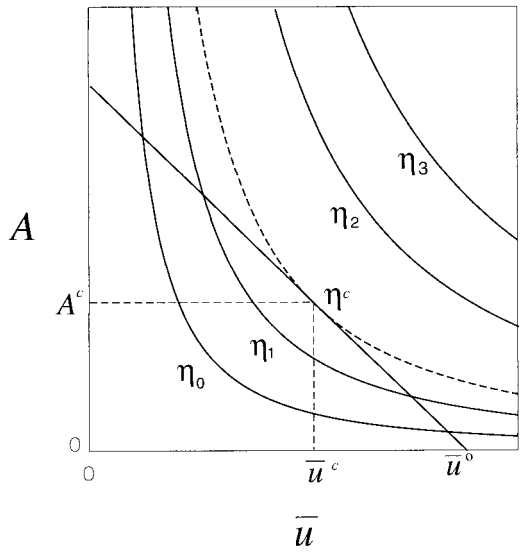

FIG. 1. Graphical derivation of A^c and $\overline{u}^c$ as in Fyfe and Held (1990). The curves represent the relationship between A and $\overline{u}$ (based on quasi-linear slowly varying theory) that must exist in a steady state for different forcing amplitudes η (where $\eta_0 < \eta_1 < \eta_2 < \eta_3$). The straight line represents the relation between A and $\overline{u}$ that exists at all times for a flow that evolves from the initial wind $\overline{u}^\circ$. The dashed curve marks the critical amplitude η^c above which no steady states can evolve from the initial wind $\overline{u}^\circ$.

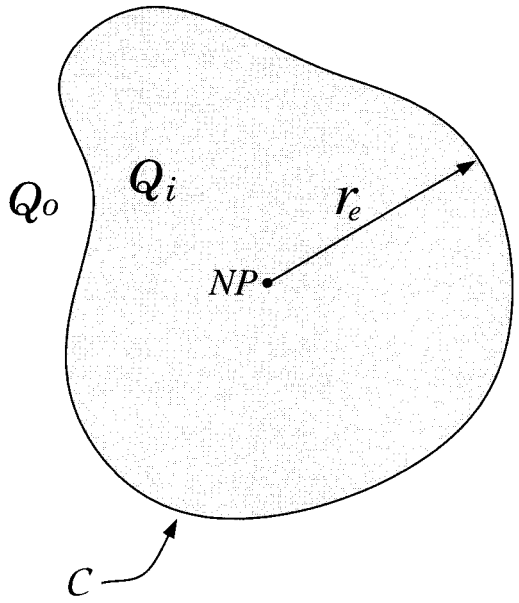

FIG. 2. Idealized vortex with uniform interior and exterior vorticity Q_i and Q_o, respectively: $\mathcal{C}$ is the bounding contour, r_e is the distance from the North Pole to $\mathcal{C}$, and NP denotes the North Pole.

geophysical waves supported in regions of extreme horizontal gradients of potential vorticity (PV), such as often associated with the polar stratospheric vortex. Consider the level view of an idealized polar stratospheric vortex shown in Fig. 2. In this example the edge of the vortex is defined by the curve $\mathcal{C}$, which separates interior and exterior regions of uniform PV, Q_i and Q_o, respectively. The PV gradient across the vortex edge is infinite and the undulations in $\mathcal{C}$ are interpreted as edge waves that have deformed the vortex from its resting state (which is, by assumption, concentric about the pole). The question we pose then is, under what conditions will these edge waves break and, in so doing, produce irreversible deformations of the vortex edge?

In this study we use the three-dimensional, quasi-geostrophic Contour Dynamics with Surgery (QG CD/CS) model developed by Dritschel and Saravanan (1994, hereafter DS) and used (with modification) by Fyfe and Wang (1997, hereafter FW) in their study of upper boundary effects on planetary wave breaking. The model uses a polar-cap f-plane geometry, meaning that the Coriolis parameter f is taken to be constant on an infinite plane that is centered at the North Pole. The initial state consists of a cylindrical PV column of radius r_o and PV jump $\Delta Q(z) \equiv Q_i(z) - Q_o(z)$, which varies with the vertical coordinate z. A vertically propagating stationary edge wave front is topographically forced, and an absorbing sponge is placed below the model's uppermost level to ensure no back reflections.

In section 2 we develop a theory for the breakdown of the vertically propagating edge waves. To obtain a reasonably simple analytical solution that reveals the basic group-velocity–mean-flow feedback mechanism in its purest form we assume an inviscid, Boussinesq, and single PV-contour fluid. The extent to which the theory is modified by the inclusion of damping effects, density variation, and multiple PV contours will remain an open question. We note, however, that there does not appear to be any major impediment to introducing these effects into the system of equations to follow [say, as was done by Dunkerton (1981) in an analogous problem for vertically propagating internal waves]. Two additional assumptions that we must make in order to obtain an analytical solution are 1) a background state that is slowly varying in height (but time dependent) upon which propagates 2) a stationary Rossby wave, sinusoidal in longitude. Fyfe and Held relaxed both 1) and 2) and found numerically that in either case the same qualitative result prevailed: there exists a threshold wind speed beyond which steady solutions are unattainable as a consequence of a runaway group-velocity–mean-flow feedback. In section 3 we numerically investigate the present system when 2) is relaxed, and leave the issue of 1) for future study. In section 4 we summarize and conclude.

2. Theory

The plan for this section is to present the wave equation for the system and then derive its dispersion relationship. Following this we use wave activity density and zonal-mean-flow equations, together with the dispersion relation, to derive a rule for edge wave breaking. We reiterate that in this model QG PV, q, is always piecewise uniform, that is, $q(z) = Q_i(z)$ inside the vortex

Unauthenticated | Downloaded 03/07/21 12:33 AM UTC

edge $\mathcal{C}$ and $q(z) = Q_o(z)$ outside and r_e is the horizontal distance from the North Pole to the vortex edge.

a. Wave equation

The linearized equation governing a small-amplitude Boussinesq disturbance streamfunction $\psi'(\lambda, r, z, t)$ to a zonally averaged mean state $\overline{\psi}(r, z, t)$ is

$$\frac{\partial q'}{\partial t} + \frac{\overline{u}}{r}\frac{\partial q'}{\partial \lambda} + \frac{\partial \overline{q}}{\partial r}v' = 0, \tag{1}$$

where

$$v'(\lambda, r, z, t) = -\frac{1}{r}\frac{\partial \psi'}{\partial \lambda}, \tag{2}$$

$$q'(\lambda, r, z, t) = \frac{1}{r}\frac{\partial}{\partial r}\left(r\frac{\partial \psi'}{\partial r}\right) + \frac{1}{r^2}\frac{\partial^2 \psi'}{\partial \lambda^2} + \frac{1}{B}\frac{\partial^2 \psi'}{\partial z^2}, \tag{3}$$

$$\overline{u}(r, z, t) = \frac{\partial \overline{\psi}}{\partial r}, \quad \text{and} \tag{4}$$

$$\overline{q}(r, z, t) = \frac{1}{r}\frac{\partial}{\partial r}\left(r\frac{\partial \overline{\psi}}{\partial r}\right) + \frac{1}{B}\frac{\partial^2 \overline{\psi}}{\partial z^2}, \tag{5}$$

where λ, r, and z are the zonal, meridional (or radial), and vertical directions, respectively. The zonal average is written as $\overline{(\,)} = 1/(2\pi)\int_0^{2\pi}(\,)\,d\lambda$ and $B = g^2/(c_p T_{\infty} f_{\delta}^2)$ (where g is gravity acceleration; c_p is specific heat capacity at constant pressure; T_{∞} a constant reference temperature; and $f_{\circ} = 2\Omega$ is the constant Coriolis parameter, with Ω being the angular rotation rate of earth). The system is nondimensionalized as in FW with timescale $S = 4\pi/f_{\circ}$, vertical length scale $H = RT_{\infty}/g$, and horizontal length scale $L = N_{\circ}H/f_{\circ}$ (R being the ideal gas constant and $N_{\circ}$ the Brunt–Väisälä frequency).

In order to make analytical progress with Eq. (1) we require that $\partial\overline{q}/\partial r$ be time invariant. In FH this was true under their assumption that the mean state was slowly varying in the meridional direction. In this study the assumed piecewise-uniform distribution of PV does not allow for slow variations in the meridional direction, so we assume a priori that

$$\frac{\partial \overline{q}}{\partial r} = \left.\frac{\partial \overline{q}}{\partial r}\right|_{t=0} = -\Delta Q(z)\delta(r - r_{\circ}), \tag{6}$$

where $\Delta Q(z) = Q_i(z) - Q_o(z)$ is the PV jump across the vortex edge and δ is the Dirac delta function. The validity of the assumption that $\partial\,\overline{q}/\partial r$ is time invariant will be judged later when we compare our theoretical predictions (given this assumption) with our numerical simulations (without this assumption).

b. Dispersion relation

To solve Eq. (1) we assume a wave solution,

$$\psi'(\lambda, r, z, t) = \tilde{\psi}(r, z)e^{i(s\lambda - \sigma t)} \quad \text{and}$$
$$q'(\lambda, r, z, t) = \tilde{q}(r, z)e^{i(s\lambda - \sigma t)}, \tag{7}$$

where s is the zonal wavenumber and σ the frequency (both constant and real). Substituting the above into Eq. (1) produces $\tilde{q} = s\overline{q}_r\tilde{\psi}/(\overline{u}s - \sigma r)$, which upon further substitution into Eq. (3) yields

$$\frac{1}{r}\frac{\partial}{\partial r}\left(r\frac{\partial \tilde{\psi}}{\partial r}\right) + \frac{1}{B}\frac{\partial^2 \tilde{\psi}}{\partial z^2} = \left(\frac{s\overline{q}_r}{\overline{u}s - \sigma r} + \frac{s^2}{r^2}\right)\tilde{\psi} \equiv V(r, z)\tilde{\psi}. \tag{8}$$

Note that this equation is time independent except parametrically through the dependence of V on $\overline{u}(r, z, t)$. We now invoke WKB theory under the assumption that V is a slowly varying function of z, that is, $V = V(r, Z)$, where $Z = \nu z$ and ν is a small dimensionless parameter. Thus, Z is a ''stretched'' variable compared to z. We now seek local wave solutions,

$$\tilde{\psi} = \Theta(r, Z)\Lambda(z, Z), \tag{9}$$

where Θ is real and Λ is complex, and which after substitution into Eq. (8) yields

$$\frac{1}{\Theta}\left[\frac{1}{r}\frac{\partial}{\partial r}\left(r\frac{\partial \Theta}{\partial r}\right) - V(r, Z)\Theta\right] = -\frac{1}{\Lambda}\left[\frac{1}{B}\frac{\partial^2 \Lambda}{\partial z^2}\right]. \tag{10}$$

Since the left-hand side is only a function of r and Z and the right-hand side only a function of z and Z, it must be the case that both sides are equal to a function of the stretched variable Z alone, say, $C(Z)$. We thus obtain the following equations:

$$\frac{1}{r}\frac{\partial}{\partial r}\left(r\frac{\partial \Theta}{\partial r}\right) - V(r, Z)\Theta - C(Z)\Theta = 0, \tag{11}$$

$$\frac{\partial^2 \Lambda}{\partial z^2} + BC(Z)\Lambda = 0. \tag{12}$$

As shown in appendix A, matching solutions at $r \neq r_{\circ}$ and $r = r_{\circ}$ leads to the following constraint on the frequency of the waves:

$$\sigma = s\left[\frac{\overline{u}_{\circ}}{r_{\circ}} - \Delta Q K_s(\sqrt{C}r_{\circ})I_s(\sqrt{C}r_{\circ})\right], \tag{13}$$

where $\overline{u}_{\circ} = \overline{u}(r_{\circ}, Z, t)$, and I_s and K_s are modified Bessel functions of the first and second kind, respectively. Now since by assumption the coefficient $C(Z)$ in Eq. (12) is slowly varying, we can use standard WKB theory (Nayfeh 1981)to obtain

$$\Lambda(z, Z) = \frac{\Lambda_{\circ}}{\sqrt{m(Z)}}\exp\left[i\int m(Z)\,dz\right], \tag{14}$$

where $\Lambda_{\circ}$ is a constant (determined from the lower boundary condition) and $m(Z)$ is the vertical wavenumber satisfying $m = \sqrt{BC}$. The dispersion relationship for the system then follows from Eq. (13), that is,

$$\sigma = s\left[\frac{\overline{u}_{\circ}}{r_{\circ}} - \Delta Q K_s\left(\frac{m}{\sqrt{B}}r_{\circ}\right)I_s\left(\frac{m}{\sqrt{B}}r_{\circ}\right)\right]. \tag{15}$$

Unauthenticated | Downloaded 03/07/21 12:33 AM UTC

Real solutions to this equation exist only when $0 < \overline{u}_\circ/(r_\circ \Delta Q) - \sigma/(s\Delta Q) < (2s)^{-1}$. Finally, the vertical group velocity, $C_g \equiv \partial\sigma/\partial m$, is given by

$$C_g = \frac{s\Delta Q r_\circ}{2\sqrt{B}} \times \left\{ I_s\left(\frac{m}{\sqrt{B}} r_\circ\right)\left[K_{s-1}\left(\frac{m}{\sqrt{B}} r_\circ\right) + K_{s+1}\left(\frac{m}{\sqrt{B}} r_\circ\right)\right] - K_s\left(\frac{m}{\sqrt{B}} r_\circ\right)\left[I_{s-1}\left(\frac{m}{\sqrt{B}} r_\circ\right) + I_{s+1}\left(\frac{m}{\sqrt{B}} r_\circ\right)\right]\right\}. \quad (16)$$

For large $x = mr_\circ/\sqrt{B}$ (i.e., small vertical wavelength, which is our WKB limit) we have, using asymptotic formulas for the modified Bessel functions, that

$$\sigma \approx s\left[\frac{\overline{u}_\circ}{r_\circ} - \frac{\Delta Q}{\pi}\left(\frac{m}{\sqrt{B}} r_\circ\right)^{-1}\right] \quad \text{and} \quad (17)$$

$$C_g \approx \frac{s\Delta Q r_\circ}{\pi\sqrt{B}}\left(\frac{m}{\sqrt{B}} r_\circ\right)^{-2} \approx \frac{s r_\circ \pi}{\Delta Q\sqrt{B}}\left(\frac{\overline{u}_\circ}{r_\circ} - \frac{\sigma}{s}\right)^2. \quad (18)$$

As can be seen, the vertical group velocity (in this limit) is proportional to the square of the Doppler-shifted zonal mean flow at $r_\circ$. This contrasts to the meridionally propagating case treated in FH where the horizontal group velocity is more weakly dependent on the zonal mean flow (i.e., is proportional to the zonal mean flow to the power of 1.5).

c. The one-half rule for edge wave breaking

We now derive a rule for edge wave breaking following the approach set out in FH. Here we work with two equations, one connecting wave activity density and zonal mean flow in the steady state, and another connecting wave activity density and zonal-mean-flow change for all time. Equating $\partial A/\partial\overline{u}$ evaluated from both these equations establishes the critical steady-state zonal mean flow.

As shown in appendix B, the wave activity density

$$A(z, t) = 2\pi\rho_\circ r_\circ^2 \Delta Q \overline{\eta'^2}|_{r_\circ} \quad (19)$$

(where $\overline{\eta'^2}|_{r_\circ}$ is the mean square displacement from $r = r_\circ$) is governed by

$$\frac{\partial A}{\partial t} + \frac{\partial}{\partial z}(C_g A) = 0. \quad (20)$$

Under steady conditions, that is, $\partial A/\partial t = 0$, it follows that $A = \beta C_g^{-1}$, where β is a constant. Given that $C_g = C_g(mr_\circ/\sqrt{B})$ [Eq. (16)] and $\overline{u}_\circ = \overline{u}_\circ(mr_\circ/\sqrt{B})$ [Eq. (15) with $\sigma = 0$] we obtain via the chain rule our first key equation:

$$\frac{\partial A}{\partial \overline{u}_\circ} = \frac{2A}{r_\circ \Delta Q \mathcal{D}\left(\frac{m}{\sqrt{B}} r_\circ\right)}, \quad (21)$$

where $\mathcal{D}$ is a complicated combination of Bessel functions (given in appendix C).

Also derived in appendix B are the following relationships between A at time t and the $\overline{u}$ change between time $t = 0$ and t [taking $A(z, 0) = 0$]:

$$A(z, t) = -4\pi\rho_\circ r_\circ^2 \int_0^\infty \Delta\overline{u}\, dr \approx 4\pi\rho_\circ r_\circ^2 \mathcal{E}(\Delta\overline{u}_\circ)^2, \quad (22)$$

where the right-hand side follows from the assumption that the vortex remains circular while displaced off the pole ($\mathcal{E}$ is an empirically derived function of ΔQ whose exact functional form is irrelevant to what follows). Taking the derivative of the right-hand side of Eq. (22) with respect to $\overline{u}_\circ$ yields our second key equation:

$$\frac{\partial A}{\partial \overline{u}_\circ} = \frac{2A}{\Delta\overline{u}_\circ}. \quad (23)$$

Equating Eq. (21) and Eq. (23) produces the equation for the critical steady-state values $\overline{u}_\circ^c$ and m^c,

$$\frac{\overline{u}_\circ^c}{r_\circ \Delta Q} - \mathcal{D}\left(\frac{m^c}{\sqrt{B}} r_\circ\right) = \frac{\overline{u}_\circ^\circ}{r_\circ \Delta Q}, \quad (24)$$

while at the same time Eq. (15) with $\sigma = 0$ yields

$$\frac{\overline{u}_\circ^c}{r_\circ \Delta Q} - K_s\left(\frac{m^c}{\sqrt{B}} r_\circ\right) I_s\left(\frac{m^c}{\sqrt{B}} r_\circ\right) = 0. \quad (25)$$

With Eqs. (24) and (25) we have two equations in the two unknowns $\overline{u}_\circ^c/(r_\circ\Delta Q)$ and $m^c r_\circ/\sqrt{B}$. We note that for large $x = mr_\circ/\sqrt{B}$ it follows from Eq. (18) (with $\sigma = 0$) that $C_g \approx (s\pi/\Delta Q\sqrt{B}\, r_\circ)\, \overline{u}_\circ^2$. Therefore, given that $A = \beta C_g^{-1}$, we have that $\partial A/\partial\overline{u}_\circ \approx -2A/\overline{u}_\circ$, which together with Eq. (23) yields

$$\frac{\overline{u}_\circ^c}{\overline{u}_\circ^\circ} \approx \frac{1}{2}. \quad (26)$$

In other words, in this asymptotic limit, a steady state is possible if, and only if, the zonal mean flow at $r_\circ$ is decelerated by less than one-half of its initial value. This contrasts with the smaller critical value of two-fifths derived by FH for the case of meridionally propagating Rossby waves.

In Fig. 3 we plot the exact (solid curve) and asymptotic (dashed line) critical ratio $\overline{u}_\circ^c/\overline{u}_\circ^\circ$ for a range of $\overline{u}_\circ^\circ(r_\circ\Delta Q)$ (for $s = 1$). Take note that no propagating wave solutions exist for $\overline{u}_\circ/(r_\circ\Delta Q) \geq 0.5$ (given $\sigma = 0$). As can be seen the exact critical ratio varies weakly with $\overline{u}_\circ^\circ/(r_\circ\Delta Q)$ and approximately converges to one-half as $\overline{u}_\circ^\circ/(r_\circ\Delta Q) \to 0$. This differs from FH in the sense

Unauthenticated | Downloaded 03/07/21 12:33 AM UTC

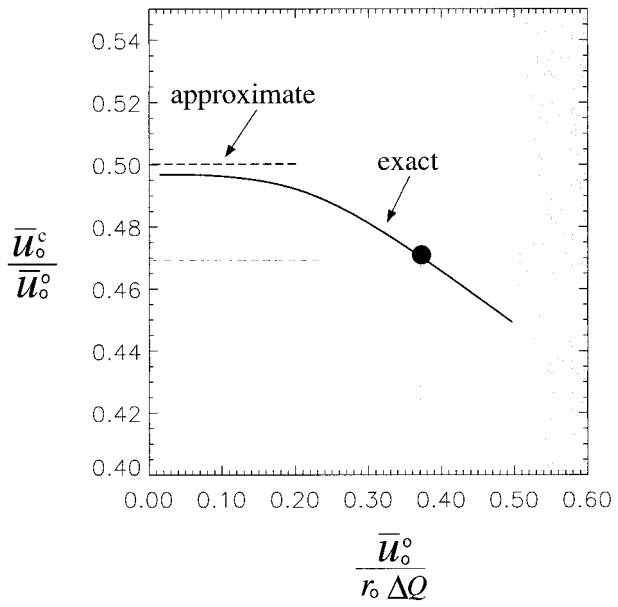

FIG. 3. Relation between the initial state as expressed by $\overline{u}^\circ_\circ(r_\circ \Delta Q)$ and the critical ratio $\overline{u}^c_\circ/\overline{u}^\circ_\circ$ (for $s = 1$). The dashed horizontal line is the approximate ratio for small $\overline{u}^\circ_\circ/(r_\circ \Delta Q)$. No propagating wave solutions exist beyond $\overline{u}^\circ_\circ/(r_\circ \Delta Q) = 0.5$ (shaded area). The solid dot identifies the initial setup and critical ratio in the numerical experiments discussed in section 3.

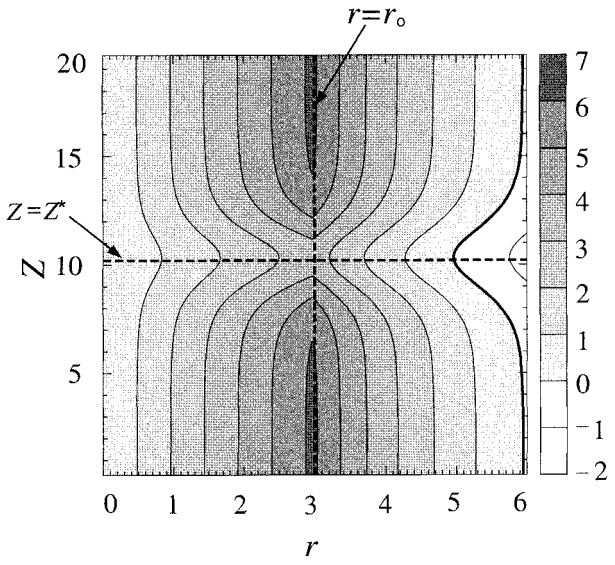

FIG. 4. The initial zonal mean wind distribution. The vertical coordinate is given by $Z = \nu z$, with z in units of scale height and $\nu = 0.1$. The zero wind line is indicated by the thick contour.

that their critical ratio is independent of the initial zonal mean flow.

3. Numerical verification

In the previous section we formulated a theory for the interaction between a vertically propagating edge wave and a vertically sheared zonal mean flow. To allow for a reasonably simple analytical solution we assumed an inviscid, Boussinesq, and single PV-contour fluid. From the point of view of obtaining analytical solutions, the introduction of damping (say, Rayleigh friction and Newtonian cooling), density variation with height, or multiple PV contours would not appear to pose a major obstacle to extending the theory. On the other hand, our other key assumptions of 1) slow variation and 2) quasilinearity cannot be relaxed and at the same time analytical solutions obtained. Both of these assumptions were numerically tested in FH and it was found that relaxing these assumptions led to the same qualitative results. Here we will test 2) and leave the question of 1) open.

a. Physical setup

To begin we set the time, vertical length, and horizontal length scales to $S = 1$ day, $H \approx 6.14$ km, and $L \approx 902$ km, respectively (in turn yielding $B \approx 1$). Further, we consider a vortex initially centered on the pole with radius $r_\circ = 3$ and PV jump ΔQ chosen so as produce an initial zonal mean wind with the hourglass distribution shown in Fig. 4. Recall that the vertical coordinate is given by $Z = \nu z$ with z in units of scale height and $\nu = 0.1$. The position of the minimum wind at each r is indicated by the horizontal dashed line at height Z^*, while the position of the maximum wind at each Z is indicated by the vertical dashed line at radius $r_\circ$. The bold contour defines the zero wind line, which since it is so far away from the vortex edge is unimportant (at least initially, as we shall see). While these zonal mean winds are meant to resemble the winter stratospheric winds, there are two notable differences: 1) the model jets line up vertically (predisposing breaking at the center point) and 2) the vertical variation is much weaker than observed owing to our use of the WKB assumption. With regard to 2) we note that while strict validity of the WKB assumption in this particular application can be questioned, it is generally accepted that it leads to ''valuable, and often quantitative'' results (Andrews et al. 1987, p. 211), and indeed it has been applied time and time again in middle-atmosphere planetary wave propagation studies (e.g., Karoly and Hoskins 1982).

In the numerical experiments to be discussed we have used 120 vertical levels yielding about 10 levels per vertical wavelength and a domain that accommodates about 12 vertical wavelengths in total (with a sponge thickness of about 3 vertical wavelengths). The results that follow are insensitive to increased vertical levels and/or domain height. To generate an upward-propagating $s = 1$ wave front we force the system with the bottom topography shown in Fig. 5 (slowly switched on in time to limit the excitation of waves with nonzero phase speed).

Unauthenticated | Downloaded 03/07/21 12:33 AM UTC

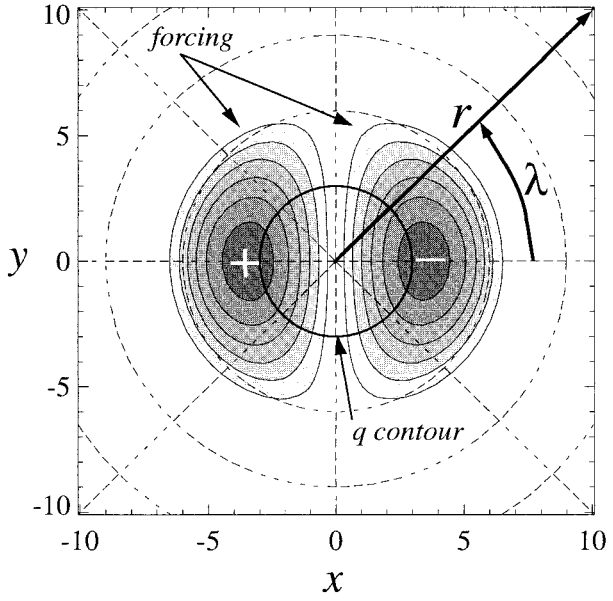

FIG. 5. Plan view of the initial polar vortex (bold circle) on an f-cap plane. The topography is shown by shaded contours. The North Pole is the center of the plot.

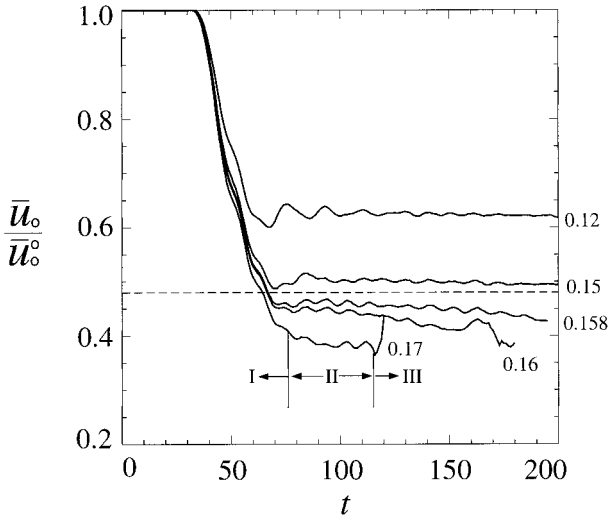

FIG. 6. The ratio $\overline{u}_\circ/\overline{u}_\circ^\circ$ evaluated at Z^* for $\eta_\circ = 0.12$, 0.15, 0.158, 0.16, and 0.17. The dashed line is the critical ratio as predicted theoretically.

b. Nonlinear numerical simulations

A series of numerical experiments over a range of topographic amplitudes have been carried out and are summarized in Fig. 6. In this figure the ratio $\overline{u}_\circ/\overline{u}_\circ^\circ$ at Z^* is plotted as a function of time for several topographic amplitudes $\eta_\circ$ (as labeled). Inspecting these curves we conclude that steady states are obtained only if $\eta_\circ \leq 0.15$, or equivalently, only if $\overline{u}_\circ/\overline{u}_\circ^\circ \geq 0.47$. For $\eta_\circ \leq 0.15$ this ratio remains unchanged when we continue the integrations up to $t = 300$ (not shown). The horizontal dashed line shows the theoretically predicted critical ratio obtained in the last section. One can see that the theoretical prediction is quite accurate in this case. For $\eta_\circ > 0.15$ the zonal mean wind decelerates beyond the theoretically predicted critical ratio and continues to slowly decelerate.

As suggested in Fig. 6, and as characterized further in the following discussion, there appear to be three phases in the evolution of the system when $\eta_\circ > 0.15$: (i) an initial phase of deceleration as the wave front passes the shear layer (as in the steady cases), (ii) an intermediate phase of small deceleration presumably involving enhanced zonal-mean-flow–group-velocity feedback, and (iii) a final rapid phase of wave breaking involving the migration of a stagnation point (i.e., a hyperbolic point of no flow) across the vortex edge. To characterize the system further, we now detail one steady and one unsteady case.

c. Steady case

Consider the $\eta_\circ = 0.12$ case shown in Fig. 6. For this case we plot in Fig. 7 contours of particle displacement from $r_\circ$, that is, $\eta'|_{r_\circ}$. One sees upward wave propagation with the waves increasing in amplitude and decreasing in vertical wavelength in the shear layer (centered at $Z = 10$). By $t = 100$ the waves have propagated into the sponge layer (above $Z = 20$) and the system has reached its steady state. Regarding the very short vertical wavelengths seen in Fig. 7, we reiterate that these experiments test the quasi-linearity assumption alone. Experiments to test the WKB assumption await future study, but we are optimistic that, as in FH, the same qualitative results will hold given more realistic vertical wavelengths.

Another perspective on the wave evolution is afforded by Fig. 8, which shows the wave activity density as a function of height and time. Note that the wave activity density plotted here is defined by Eq. (B1) (appendix B) and is normalized by $\eta_\circ^2$. As expected from the group velocity expression the wave front slows as it approaches the shear layer (as indicated by the tilting of the isolines around $Z = 10$). Plots of the zonal mean flow (not shown) reveal that as the wave front propagates upward it leaves a trail of decelerated wind behind with the largest deceleration occurring at the initial vortex edge and in the middle of the shear layer (where the vortex displacement is greatest).

d. Unsteady case

Now consider the $\eta_\circ = 0.16$ case also shown in Fig. 6. For this stronger forcing the zonal mean wind at Z^* decelerates beyond the critical value and, as such, the system cannot achieve a steady state. A perspective view of the vortex at $t = 166$ is shown in Fig. 9. Within the shear layer the vortex has begun to filament (i.e., break in terms of irreversibility) but not to such an extent that continued upward propagation is suppressed in any sig-

Unauthenticated | Downloaded 03/07/21 12:33 AM UTC

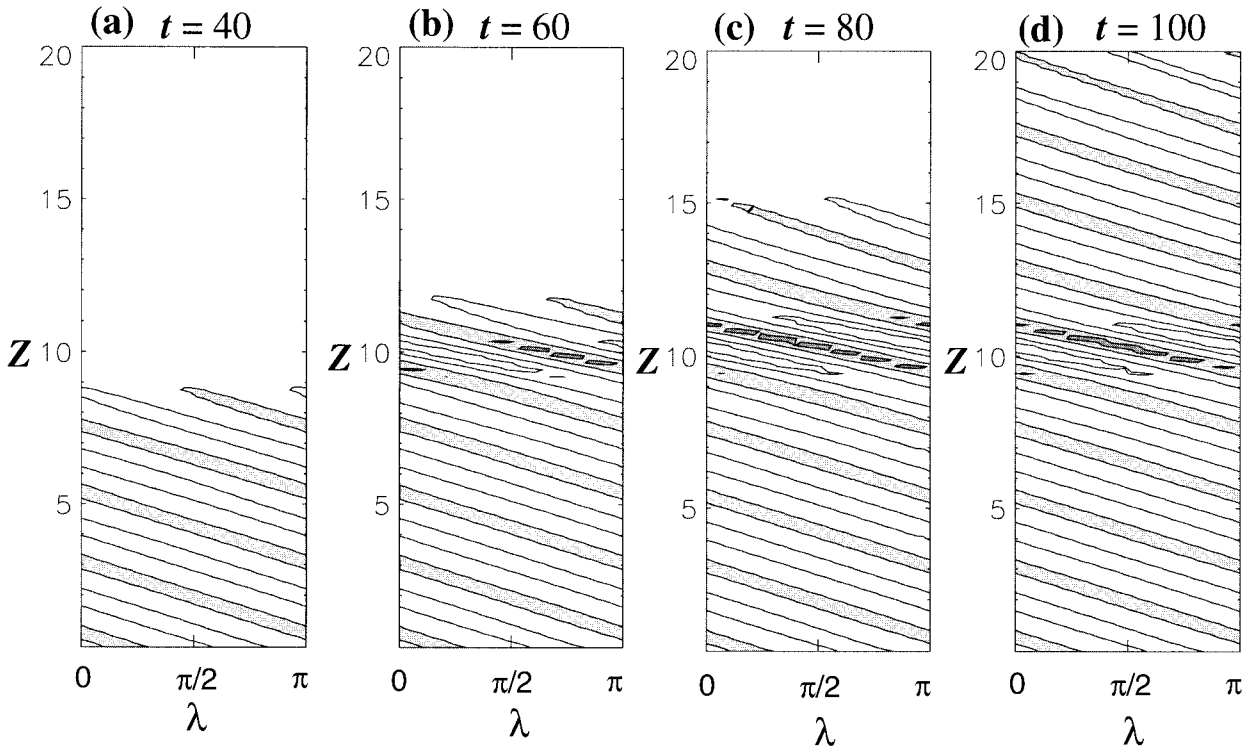

FIG. 7. Particle displacement contours for $\eta_o = 0.12$ at (a) $t = 40$, (b) $t = 60$, (c) $t = 80$, and (d) $t = 100$. The shaded and unshaded contours represent positive and negative values, respectively. The contour interval is 0.5.

nificant way. Dritschel and Saravanan (1994) and FW both show that continued local breaking of this sort will eventually inhibit vertical propagation given sufficient PV homogenization.

Figure 10 shows the sequence of events leading to this distortion (at Z^*). Following local overturning of the PV contour (Fig. 10a) a thin filament stretches outside and around the vortex (Fig. 10b) and then separates (Fig. 10c). The filament then orbits the vortex until it is eventually surgically removed (Fig. 10d). Similar cycles of overturning, thinning, separation, and expulsion follow at intervals of approximately 14 days. A similar process was observed by Polvani and Plumb (1992) for a two-dimensional perturbed vortex.

It has been observed that the initial overturning involves the migration of a stagnation point across the contour. This is shown in Figs. 11a,b, where the solid dot indicates the stagnation point and velocity vectors are indicated with arrows. Following the initial passage of the wave front and before $t = 150$ (not shown) the PV contour slowly shifts toward the lower-left quadrant of the domain without significant departure from its initial circular shape (with the stagnation point being located well outside the contour). After $t \approx 150$, a region of high curvature builds on the contour (Fig. 11a) and when it becomes sufficiently high the contour overturns. At precisely this time the stagnation moves inside the contour (Fig. 11b). The strain field around the stagnation point is shown in Figs. 11c,d. As can be seen, once the stagnation point crosses the contour, part of the contour is drawn toward an area of large negative strain and is subsequently stretched out. Polvani et al. (1989) also found that the onset of filamentation is associated with a stagnation point migrating inside a vortex (in their simplier two-dimensional system).

4. Summary and discussion

In this paper we have investigated the interaction between a vertically propagating planetary-scale edge wave front and a vertically sheared zonal mean flow (initially free of any critical levels). The inviscid, Boussinesq, single PV-contour, quasi-linear, and slowly varying theory that we have developed shows that if the zonal mean wind decelerates by less than roughly one-half its initial value, a steady state will ensue. On the other hand, if the deceleration exceeds one-half its initial value, no steady state is obtained. Numerical simulations with a fully nonlinear CD/CS model show that despite the simplifying quasi-linear assumption the prediction of a one-half threshold is a good one (over the range of parameters considered). The numerical model also shows that when the threshold is exceeded wave breaking eventually occurs in the shear region through a process involving the migration of a stagnation point across the vortex edge.

We repeat that to obtain a reasonably simple analytical solution we have assumed an inviscid, Boussinesq,

Unauthenticated | Downloaded 03/07/21 12:33 AM UTC

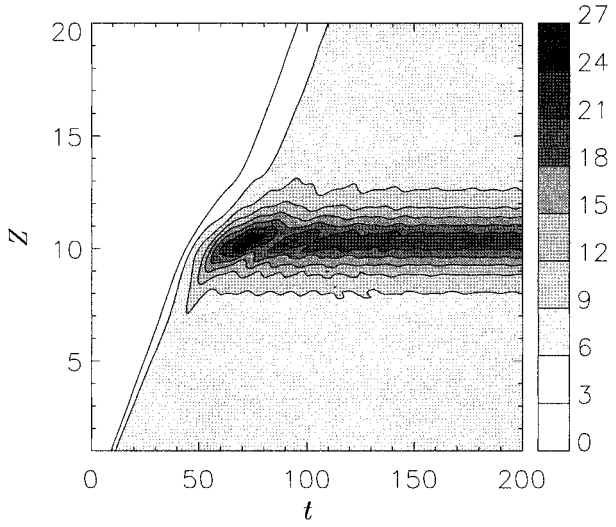

FIG. 8. Wave activity density A (normalized by $\eta_\circ^2$) for $\eta_\circ = 0.12$.

and single PV-contour fluid. We see no major obstacle, though, to extending the theory by introducing damping (say, Rayleigh friction and Newtonian cooling), density variation with height, and multiple PV contours. On the other hand, the slowly varying assumption cannot be relaxed and at the same time analytical solutions obtained. We remain optimistic though that, as in FH, our results will remain qualitatively correct when strict validity of the WKB assumption is not ensured.

Acknowledgments. The authors are grateful to M. Holzer, G. Flato, and J. Scinocca for helpful review comments. We are also grateful to R. Mo for many useful discussions. Funding for this research is through the Climate Research Network of the Atmospheric Research Service.

APPENDIX A

Solution to Eq. (11)

a. Case: $r \neq r_\circ$

Equation (11) is singular at $r_\circ$ because of the δ-function behavior of $\overline{q}_r$ [recall the definition of V in Eq. (8)]. Away from $r_\circ$ where $\overline{q}_r$ is zero Eq. (11) is a modified Bessel equation whose general solution is

$$\Theta(r, Z) = C_1 I_s(\sqrt{C}r) + C_2 K_s(\sqrt{C}r), \qquad \text{(A1)}$$

where C_1 and C_2 are, at this point, unknown functions of Z (I_s and K_s are modified Bessel functions of the first and second kind, respectively). Note that $I_s(\sqrt{C}r) \to \infty$ as $r \to \infty$ and $K_s(\sqrt{C}r) \to \infty$ as $r \to 0$. Demanding that Θ be bounded as $r \to \infty$ and $r \to 0$ produces two solution branches for Θ, that is, one where $C_1 = 0$ for $r > r_\circ$ and another where $C_2 = 0$ for $r < r_\circ$. Matching the two branches of Θ as $r \to r_\circ$ yields $C_1 = B_s K_s\ (\sqrt{C}r_\circ)$ and $C_2 = B_s I_s(\sqrt{C}r_\circ)$. Thus we have

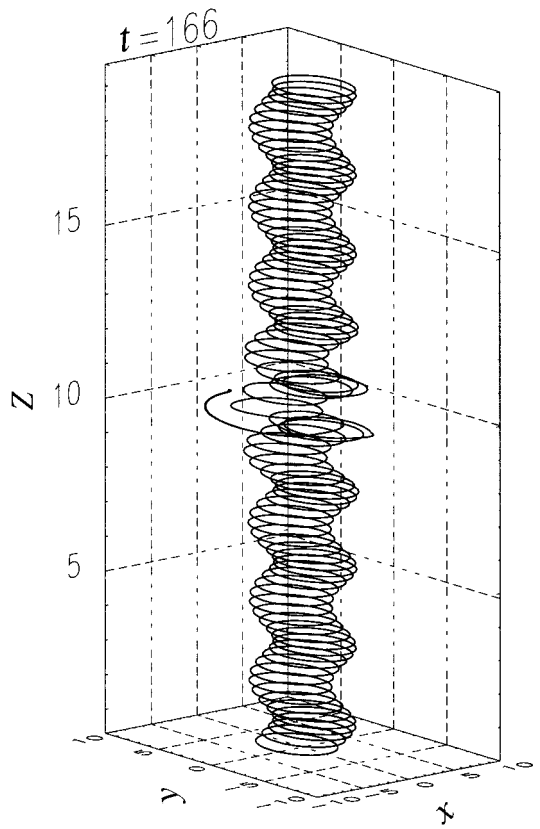

FIG. 9. Perspective view of the vortex at $t = 166$ for $\eta_\circ = 0.16$.

$$\Theta(r, Z) = \begin{cases} B_s K_s(\sqrt{C}r_\circ) I_s(\sqrt{C}r) & r < r_\circ, \\ B_s I_s(\sqrt{C}r_\circ) K_s(\sqrt{C}r) & r > r_\circ, \end{cases} \qquad \text{(A2)}$$

where B_s is obtained from the following normalization constraint $\int_0^\infty r\Theta^2\, dr = 1$:

$$B_s^2 = \frac{8}{r_\circ^2 [I_s^2(\sqrt{C}r_\circ) X^2 - K_s^2(\sqrt{C}r_\circ) Y^2]}, \qquad \text{(A3)}$$

where

$$X = K_{s-1}(\sqrt{C}r_\circ) + K_{s+1}(\sqrt{C}r_\circ) \quad \text{and}$$

$$Y = I_{s-1}(\sqrt{C}r_\circ) + I_{s+1}(\sqrt{C}r_\circ).$$

b. Case: $r = r_\circ$

We now return to the general equation (11), which is valid for all r, including $r_\circ$. As noted, Eq. (11) is singular at $r_\circ$ because of the δ-function behavior of $\overline{q}_r$. To find the so-called jump condition that ensures that Θ in Eq. (A2) solves Eq. (11) at $r_\circ$ we apply the operator

$$\lim_{\epsilon \to 0} \int_{r_\circ - \epsilon}^{r_\circ + \epsilon} r(\,)\, dr$$

Unauthenticated | Downloaded 03/07/21 12:33 AM UTC

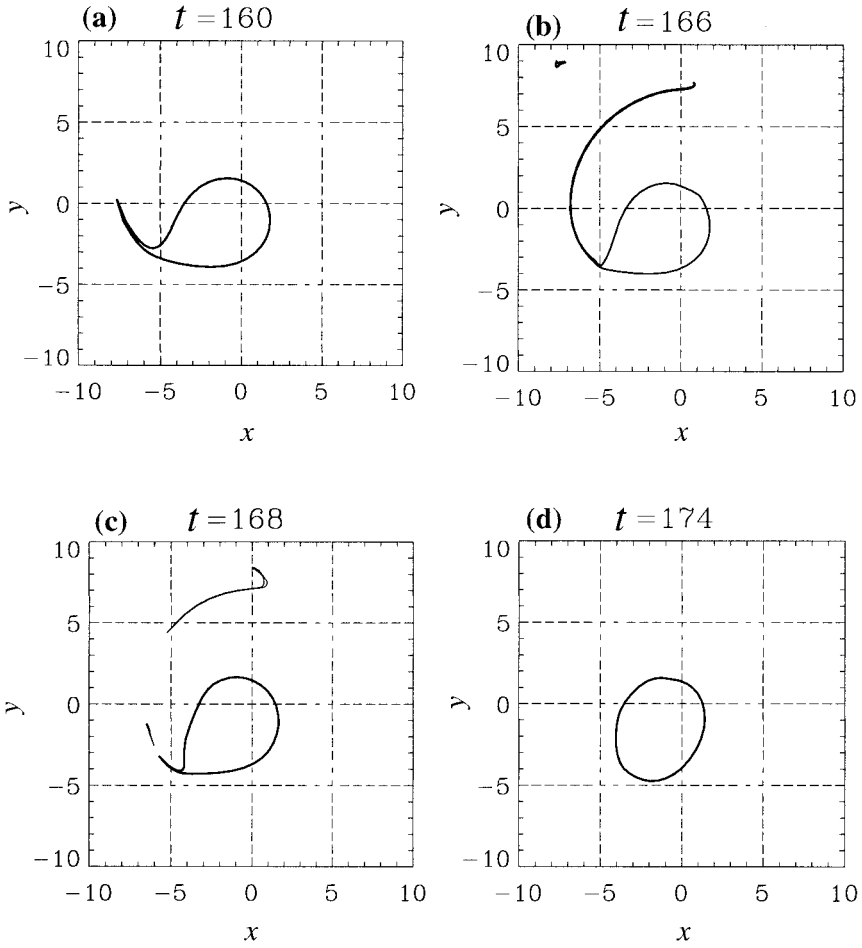

FIG. 10. The PV contour at Z^* for $\eta_\circ = 0.16$ at (a) $t = 160$, (b) $t = 166$, (c) $t = 168$, and (d) $t = 174$.

to Eq. (11) (Yih 1980). Here ϵ is a small real number. This yields (after some manipulation)

$$\lim_{\epsilon \to 0} \left[r \frac{\partial \Theta}{\partial r} \right]_{r_\circ - \epsilon}^{r_\circ + \epsilon} = - \frac{s r_\circ \Delta Q}{\overline{u}_\circ s - \sigma r_\circ} \Theta_\circ, \tag{A4}$$

where $\overline{u}_\circ = \overline{u}(r_\circ, Z, t)$ and $\Theta_\circ = \Theta(r_\circ, Z)$. Using Θ from Eq. (A2) in the above yields Eq. (11).

APPENDIX B

Wave Activity Density

As shown in DS the wave activity density for this one PV-contour system is

$$A(z, t) = \frac{1}{4} \rho_\circ \Delta Q \oint_C (r^2 - r_\circ^2)^2 \, d\lambda, \tag{B1}$$

assuming that the contour is not displaced over the pole (as in this study). Defining $\eta' \equiv r - r_\circ$ then to first order A is given by Eq. (19).

a. Derivation of Eq. (20)

Multiplying the particle displacement equation $\partial \eta'/\partial t + (\overline{u}/r)\partial \eta'/\partial \lambda = v'$ (Andrews et al. 1987) by $4\pi \rho_\circ r_\delta^2 \eta' \Delta Q$ and zonally averaging along $r_\circ$ yields

$$\frac{\partial A}{\partial t} - 4\pi \rho_\circ r_\delta^2 \Delta Q \overline{v' \eta'}|_{r_\circ} = 0. \tag{B2}$$

Similarly, using the Eliassen–Palm flux equation $\nabla \cdot \mathbf{S} = -\rho_\circ r \overline{v' q'}$, where $\mathbf{S} = [S^{(\lambda)}, S^{(r)}, S^{(z)}] = [0, -\rho_\circ r \overline{u' v'}, -(\rho_\circ r/B) \overline{v' \partial \psi'/\partial z}]$ (Andrews et al. 1987), we get

$$\frac{\partial S}{\partial z} + 4\pi \rho_\circ r_\delta^2 \Delta Q \overline{v' \eta'}|_{r_\circ} = 0, \tag{B3}$$

where $S \equiv 4\pi \int_0^\infty r S^{(z)} \, dr$. To obtain this equation we used $\overline{u' v'} = 0$ (for a single wave as here) and $\int_0^\infty r^2 \overline{v' q'} \, dr = r_\delta^2 \Delta Q \overline{v' \eta'}|_{r_\circ}$ [following from known properties of the δ function as shown in Wang (1998)]. Adding Eqs. (B2) and (B3) gives

$$\frac{\partial A}{\partial t} + \frac{\partial S}{\partial z} = 0. \tag{B4}$$

Unauthenticated | Downloaded 03/07/21 12:33 AM UTC

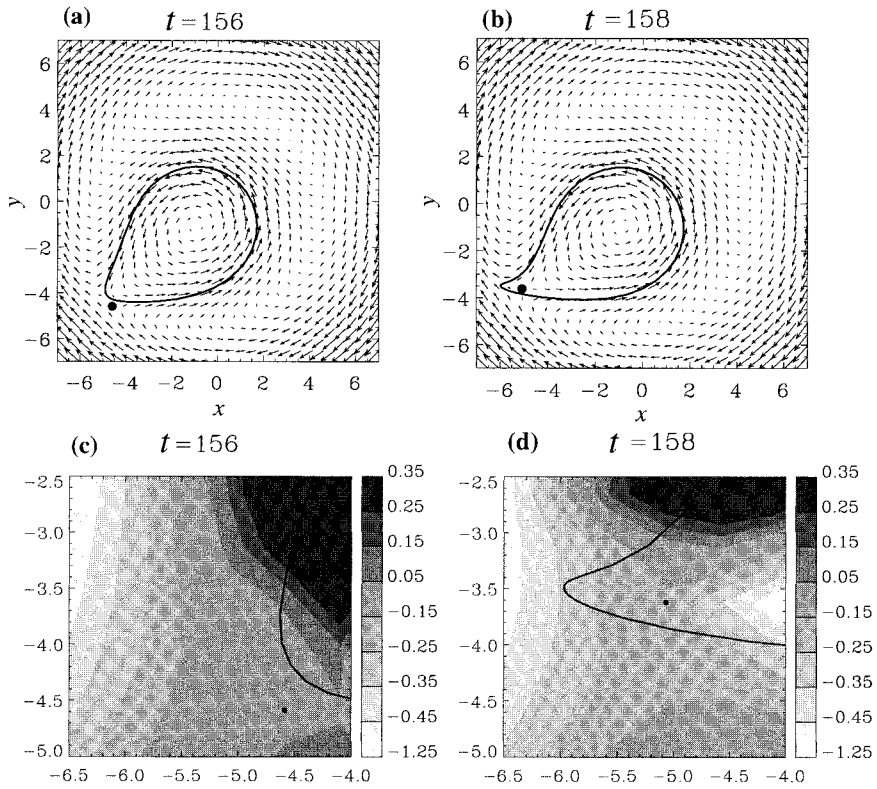

FIG. 11. The PV contour, velocity, and stagnation point (solid dot) at Z^* for $\eta_\circ = 0.16$ at (a), (c) $t = 156$ and (b), (d) $t = 158$. (a), (b) Arrows represent the velocity field; (c), (d) shaded contours are the strain field.

We now relate A and S. Using $\eta' = \tilde{\eta}e^{i(s\lambda-\sigma t)}$ and $v' = -is\psi'/r$ in the particle displacement equation gives $\overline{\eta'^2} = 0.5s^2\overline{\psi'^2}|_r/(\sigma r_\circ - \overline{u}_\circ s)^2$. Also $\overline{\psi'^2} = 0.5\Theta^2|\Lambda|^2 = 0.5B_s^2K_s^2(\sqrt{C}r_\circ)\, I_s^2(\sqrt{C}r_\circ)|\Lambda|^2$ and $\sigma r_\circ - \overline{u}_\circ s = -sr_\circ\Delta Q K_s(\sqrt{C}r_\circ)I_s(\sqrt{C}r_\circ)$ so

$$A = \frac{\pi\rho_\circ B_s^2|\Lambda|^2}{\Delta Q}.$$

As for S, we note that $v' = -is\psi'/r$, $\partial\psi'/\partial z = im\psi'$ and $\overline{\psi'^2} = 0.5\Theta^2|\Lambda|^2$ yield

$$S = \frac{2\pi\rho_\circ sm}{B}|\Lambda|^2,$$

where the $\int_0^\infty r\Theta^2\, dr = 1$ normalization has been used. With these expressions for A and S and replacing B_s^2 by Eq. (A3), it follows that

$$S = \frac{r_\circ^2\Delta Q sm}{4B} \times \left\{ I_s^2\left(\frac{m}{\sqrt{B}}r_\circ\right)\left[K_{s-1}\left(\frac{m}{\sqrt{B}}r_\circ\right) + K_{s+1}\left(\frac{m}{\sqrt{B}}r_\circ\right)\right]^2 - K_s^2\left(\frac{m}{\sqrt{B}}r_\circ\right)\left[I_{s-1}\left(\frac{m}{\sqrt{B}}r_\circ\right) + I_{s+1}\left(\frac{m}{\sqrt{B}}r_\circ\right)\right]^2\right\}A.$$

Manipulation of the Bessel functions and group velocity expression in Eq. (16) yields $S = C_gA$, which together with Eq. (B4) produces Eq. (20).

b. Derivation of Eq. (22)

Integrating $\partial\overline{u}/\partial t = -\overline{v'q'}$ [Andrews et al. (1987), with the residual mean term neglected) with $\int_0^\infty \overline{v'q'}\, dr = \Delta Q\overline{v'\eta'}|_{r_\circ}$ [following from known properties of the δ function as shown in Wang (1998)] yields

$$\frac{\partial}{\partial t}\int_0^\infty \overline{u}\, dr = -\Delta Q\overline{v'\eta'}|_{r_\circ}. \tag{B5}$$

This equation, together with Eq. (B2) and after time integration with $A(z, 0) = 0$, produces the left-hand side of Eq. (22). It now remains to relate the radially integrated mean zonal flow change and the mean zonal flow change at $r_\circ$. Let us assume that the passing wave front shifts the vortex off the pole with the vortex remaining circular with centroid located distance ϵ from the North Pole. Numerical experimentation (not shown) reveals this to be acceptable given reasonably small (albeit finite amplitude) displacements of the vortex. As shown in Wang (1998) this idealization allows us to write

Unauthenticated | Downloaded 03/07/21 12:33 AM UTC

$$\Delta\overline{u} = \begin{cases} 0 & \text{for } r \le r_\circ - \epsilon, \\ -\dfrac{(\pi r^2 - a)\Delta Q}{2\pi r} & \text{for } r_\circ - \epsilon < r \le r_\circ, \\ -\dfrac{(\pi r_\circ^2 - a)\Delta Q}{2\pi r} & \text{for } r_\circ < r \le r_\circ + \epsilon, \\ 0 & \text{for } r > r_\circ - \epsilon, \end{cases} \tag{B6}$$

where the area common to the initial and shifted vortices is $a = \pi r_\delta^2 + r^2(\beta - \beta') - \epsilon r \sin\beta$ with $\cos\beta = (r^2 + \epsilon^2 - r_\delta^2)/2r\epsilon$ and $\cos\beta' = (r^2 - \epsilon^2 - r_\delta^2)/2\, r_\circ\epsilon$. Inspecting this expression shows that shifting a circular vortex off the pole results in maximum deceleration at $r = r_\circ$ that increases with increasing ϵ. Further, it is shown in Wang (1998) that to very good approximation

$$\int_0^\infty \Delta\overline{u}\, dr \approx -\mathcal{E}(\Delta\overline{u}_\circ)^2, \tag{B7}$$

where $\mathcal{E}$ is functionally related to ΔQ.

APPENDIX C

Bessel Functions: $\mathcal{D}(x)$

$$\begin{aligned} \mathcal{D}(x) = \{&[I_{s-1}(x) + I_{s+1}(x)]K_s(x) \\ &- I_s(x)[K_{s-1}(x) + K_{s+1}(x)]\}^2 \\ \div \{&[I_{s-1}(x) + I_{s+1}(x)][K_{s-1}(x) + K_{s+1}(x)] \\ &- 2I_s(x)K_s(x) - 0.5I_s(x)[K_{s-2}(x) + K_{s+2}(x)] \\ &- 0.5K_s(x)[I_{s-2}(x) + I_{s+2}(x)]\}. \end{aligned}$$

REFERENCES

Andrews, D. G., J. R. Holton, and C. B. Leovy, 1987: *Middle Atmosphere Dynamics.* Academic Press, 489 pp.

Dritschel, D. G., and R. Saravanan, 1994: Three-dimensional quasi-geostrophic contour dynamics with an application to stratospheric vortex dynamics. *Quart. J. Roy. Meteor. Soc.*, **120,** 1267–1297.

Dunkerton, T. J., 1981: Wave transience in a compressible atmosphere. Part I: Transient internal wave, mean-flow interaction. *J. Atmos. Sci.*, **38,** 281–297.

Fyfe, J., and I. M. Held, 1990: The two-fifths and one-fifth rules for Rossby wave breaking in the WKB limit. *J. Atmos. Sci.*, **47,** 697–706.

——, and X. Wang, 1997: Upper-boundary effects in a Contour Dynamics/Surgery model of the polar stratospheric vortex. *Atmos.–Ocean*, **35,** 189–207.

Karoly, D. J., and B. J. Hoskins, 1982: Three-dimensional propagation of planetary waves. *J. Meteor. Soc. Japan,* **60,** 109–123.

Killworth, P. D., and M. E. McIntyre, 1985: Do Rossby-wave critical layers absorb, reflect or over reflect? *J. Fluid Mech.*, **161,** 449–492.

Nayfeh, A. H., 1981: *Introduction to Perturbation Techniques.* John Wiley and Sons, 519 pp.

Polvani, L. M., and R. A. Plumb, 1992: Rossby wave breaking, microbreaking, filamentation, and secondary vortex formation: The dynamics of a perturbed vortex. *J. Atmos. Sci.*, **49,** 462–476.

——, N. J. Zabusky, and G. R. Flierl, 1989: Filamentation of coherent vortex structures via separatrix crossing: A quantitative estimate of onset time. *Phys. Fluids*, **1A,** 181–184.

Wang, X., 1998: Onset of planetary wave breaking in a model of the polar stratospheric vortex. Ph.D. dissertation, University of Victoria, 98 pp.[Available from University of Victoria, P.O. Box 1700 STN CSC, Victoria, BC V8W 2Y2, Canada.]

Warn, T., and H. Warn, 1976: On the development of a Rossby wave critical level. *J. Atmos. Sci.*, **33,** 2021–2024.

——, and ——, 1978: The evolution of a nonlinear critical level. *Stud. Appl. Math.*, **59,** 37–71.

Yih, C. S., 1980: *Stratified Flows.* Academic Press, 418 pp.

Unauthenticated | Downloaded 03/07/21 12:33 AM UTC